ACS APPLIED MATERIALS & INTERFACES

Letter

www.acsami.org

Targeted Delivery of 5-Aminolevulinic Acid by Multifunctional Hollow Mesoporous Silica Nanoparticles for Photodynamic Skin Cancer Therapy

Xing Ma,[†] Qiuyu Qu,[†] and Yanli Zhao*[,†,‡]

[†]Division of Chemistry and Biological Chemistry, School of Physical and Mathematical Sciences, Nanyang Technological University, 21 Nanyang Link, Singapore 637371

[‡]School of Materials Science and Engineering, Nanyang Technological University, 50 Nanyang Avenue, Singapore 639798

Supporting Information

ABSTRACT: 5-Aminolevulinic acid (5-ALA) is a precursor of a strong photosensitizer, protoporphyrin IX (PphIX), for photodynamic therapy (PDT). Developing appropriate delivery carriers that can assist 5-ALA in bypassing the lipophilic barrier to directly enter into cancer cells is a research focus. The improved delivery of 5-ALA is even important for skin cancer therapy through PDT process. In this work, targeting ligand folic acid (FA)-functionalized hollow mesoporous silica nanoparticles (HMSNPs) were fabricated to deliver 5-ALA for PDT against B16F10 skin cancer cells. The FA targeting ligand enabled selective endocytosis of 5-ALA loaded HMSNPs into cancer cells. PphIX formed from delivered 5-ALA exhibited high photocytotoxicity to the cancer cells in vitro.

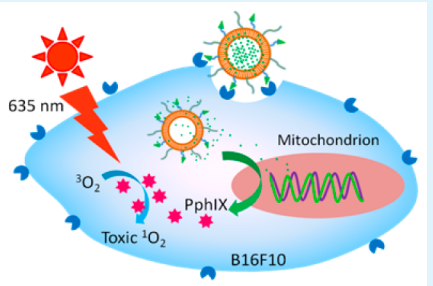

KEYWORDS: *aminolevulinic acid, hollow mesoporous silica nanoparticles, photodynamic therapy, skin cancer, targeted delivery*

Photodynamic therapy (PDT) is a palliative cancer therapeutic technique that has attracted great attention because of its noninvasive property, minimal side effects, and nontoxic components used.[1] The PDT process usually requires three components, including light, oxygen, and photosensitizers. Upon accumulation of photosensitizers in cancer cells or tumor tissues, light irradiation of proper wavelength provides energy for photosensitizers to convert surrounding oxygen ($^3O_2$) into singlet oxygen ($^1O_2$), a type of reactive oxygen species (ROS). $^1O_2$ is highly toxic and can induce apoptosis or necrosis of tumor cells, achieving cancer cell killing effect.[2−4] In the past two decades, many types of photosensitizers have been developed and explored,[5] among which 5-aminolevulinic acid (5-ALA) is widely used for PDT because it is nontoxic and can be quickly excreted from biological systems.[6] Essentially, 5-ALA is distinguished from other photosensitizers, since it is not a photosensitizer. It is a precursor for haem group synthesis in a cell organ, mitochondrion, where it is further converted to a strong photosensitizer, protoporphyrin IX (PphIX), to accomplish the functions of PDT. PphIX is also a photosensitive fluorescent molecule, which has different degradation rates in normal cells and cancer cells. Such an interesting property makes PphIX an important fluorescent label to detect cancer cells or tumor tissues.[7,8] Thus, various strategies of using nanocarriers to deliver PphIX into cancer cells have been developed for PDT.[9,10] Because of all these factors, 5-ALA serves as very attractive species for PDT, and previous studies have revealed that the administration of 5-ALA in a large amount can successfully suppress solid tumor when giving sufficient oxygen supply.[11,12]

Despite all the advantages of 5-ALA, because of its hydrophilic property and low specificity to cancer cells, limitations such as low bioavailability and poor cell permeability still hamper its practical applications for PDT.[6,13] In addition, widely existing bacteria in the biological environment might engulf 5-ALA during its administration.[14] Hence, there is a need of developing appropriate delivery vehicles that can assist 5-ALA to bypass lipophilic barrier to directly enter into cancer cells, thus protecting 5-ALA from being engulfed by bacteria. For instance, cationic gold nanoparticles[15] and self-assembled polymer nanoparticles[16,17] were developed for 5-ALA delivery. Nevertheless, developing efficient nanocarriers for 5-ALA delivery is still under exploration, and improved delivery of 5-ALA is even important for skin cancer therapy through PDT process.

Applying mesoporous silica nanoparticles (MSNPs) in biological field has been successfully proven their superiority, including good biocompatibility, high surface area and high pore volume, allowing for a large amount of drug loading and easy chemical modifications.[18] In particular, hollow mesoporous silica nanoparticles (HMSNPs) show enhanced performance for drug delivery given by highly permeable porous shells.[19] Previous research work reported that HMSNPs could enhance the loading capacity of anticancer drug doxorubicin by 100% as compared with normal MSNPs, further minimizing the toxicity of the carriers.[20] Both in vitro and in vivo studies were

Received: April 9, 2015
Accepted: May 14, 2015
Published: May 14, 2015

DOI: 10.1021/acsami.5b03087
ACS Appl. Mater. Interfaces 2015, 7, 10671−10676

carried out by using HMSNPs for anticancer drug delivery.[19] With these advantages, HMSNPs stand out as an ideal candidate for targeted delivery of 5-ALA.

Herein, we designed and fabricated a multifunctional HMSNP for targeted delivery of 5-ALA, aiming at PDT against skin cancer. To the best of our knowledge, this is the first example to use mesoporous silica for 5-ALA delivery. In addition to a large amount of 5-ALA loading, the nanochannels in the shells of HMSNPs could facilitate the 5-ALA release after entering into cancer cells, leading to quick accumulation of formed PpIX as an excellent photosensitizer for PDT (Scheme 1). To achieve high usage efficiency of the

Scheme 1. Schematic Illustration of Multifunctional HMSNP based 5-ALA Delivery for Targeted PDT in Skin Cancer Treatment

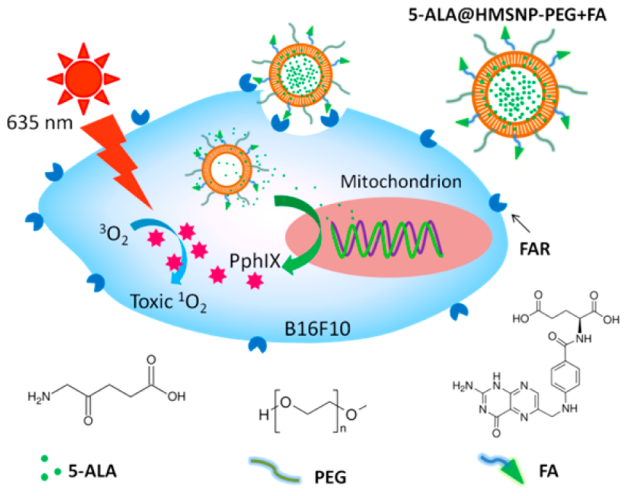

administered 5-ALA and reduce possible side effects due to nontargeted delivery, folic acid was functionalized onto the HMSNPs. Folic acid is a widely used cancer-targeting ligand, which has high affinity to folic acid receptor (FAR), a glycosyl-phosphatidyinositol-linked protein overexpressed on the surface of most cancer cells.[21] Once folic acid interacts with FAR, it facilitates the internalization of multifunctional HMSNPs into cancer cells through a nondestructive endosomal route.[19,20] In addition, biocompatible polyethylene glycol (PEG) polymer was also functionalized onto HMSNPs in order to further enhance its biocompatibility and prolong its blood circulation time, the two factors that are critical for future clinic applications.[22]

HMSNPs were prepared by a selective etching method according to previous report with minor modifications.[23] The morphology of the as-prepared HMSNPs was characterized by field emission scanning electron microscopy (FE-SEM) and transmission electron microscopy (TEM). As shown from FE-SEM image (Figure 1a), HMSNPs have a spherical shape with uniform nanoparticle size.[19,20] The diameter of HMSNPs was estimated to be around 150 nm by randomly counting 20 nanoparticles from TEM image (Figure 1b). This size is suitable for intracellular drug delivery by considering the enhanced permeability and retention (EPR) effect.[24] The structure of HMSNPs was clearly evidenced by TEM image (Figure 1c), showing empty hollow core and mesoporous shell with uniform shell thickness of about 30 nm. Perpendicular nanochannels connecting to the internal core were clearly

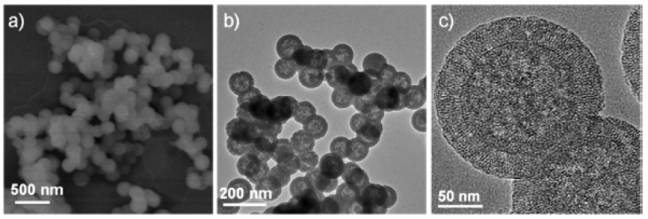

Figure 1. (a) FE-SEM image, (b) TEM image at low magnification, and(c) TEM image at high magnification of as-prepared HMSNPs.

observed, which are beneficial for the loading and release of 5-ALA.

The multifunctionalization on HMSNPs was carried out after confirming the structure and morphology of the as-prepared HMSNPs. First, HMSNPs were modified with primary amine by a grafting method. Typically, HMSNPs were suspended in ethanol solution containing (3-aminopropyl)triethoxysilane (APTES) under stirring for 48 h to yield primary amine grafted HMSNPs, noted as HMSNP-NH_2. Then, folic acid and PEG were conjugated onto HMSNP-NH_2 via 1-ethyl-3-(3-(dimethylamino)propyl)carbodiimide (EDC) and *N*-hydroxysuccinimide (NHS) coupling chemistry,[25] affording multifunctional HMSNPs, noted as HMSNP-PEG+FA. The functionalization process was characterized by FT-IR spectra (Figure S1 in the Supporting Information). In the FT-IR spectrum of HMSNP-NH_2, a new peak at 1520 cm^{-1} appeared on account of amine group stretching,[26] indicating the successful grafting of amine group onto HMSNPs. As for HMSNP-PEG+FA, the peak for amine group at 1520 cm^{-1} disappeared because of amide bond formation.[25] Considering limited molar ratio of −CH− unit in folic acid molecule, obvious peaks at 1464 and 1344 cm^{-1} attributed to the −CH− bending and 2934 cm^{-1} due to −CH− stretching indicate the presence of PEG.[27] Furthermore, a UV−vis absorbance peak at 285 nm corresponding to folic acid suggests that folic acid molecule was indeed integrated into HMSNP-PEG+FA (Figure S2 in the Supporting Information).[28]

The amount of functional groups was quantified by thermogravimetric analysis (TGA, Figure S3 in the Supporting Information). The weight loss of HMSNPs was found to be 7 wt %, and that of HMSNP-NH_2 was 12.5 wt % at 600 °C. The extra 5.5 wt % loss should be due to grafted primary amine, which was calculated to be 0.948 mmol g^{-1}. By comparing the weight loss (22.5 wt %) of HMSNP-PEG+FA with that of HMSNP-NH_2, the extra weight loss of 10 wt % further certified the successful conjugation of folic acid and PEG. Then, 5-ALA was loaded into the nanocarriers by stirring an ethanol solution containing 5-ALA (5 mg mL^{-1}) and HMSNP-PEG+FA (5 mg mL^{-1}) for 24 h. The obtained 5-ALA loaded HMSNP-PEG +FA, noted as 5-ALA@HMSNP-PEG+FA, was collected by centrifugation and then air-dried at room temperature. The further increase in weight loss (3.4 wt %) from 5-ALA@HMSNP-PEG+FA as compared with that of HMSNP-PEG+FA could be explained by the degradation of 5-ALA loaded inside 5-ALA@HMSNP-PEG+FA. Thus, the 5-ALA loading capacity was estimated to be 3.4 wt %.

N_2 adsorption/desorption measurement was carried out to further characterize the hollow and mesoporous features of all the prepared HMSNPs (Figure S4 in the Supporting Information). Typical type IV isotherms were observed for HMSNPs, HMSNP-NH_2, and HMSNP-PEG+FA.[20] Because of grafted primary amine on HMSNPs, the Brunauer−Emmett−

DOI: 10.1021/acsami.5b03087
ACS Appl. Mater. Interfaces 2015, 7, 10671−10676

Teller (BET) surface area (Table 1) decreased from 991.92 m^2 g^{-1} (HMSNPs) to 690.00 m^2 g^{-1} (HMSNP-NH_2). The BET surface area further decreased to 535.71 m^2 g^{-1} after folic acid and PEG conjugation. Thus, all the three samples showed mesoporous structure, demonstrated by the similar isotherms. Moreover, obvious hysteresis loops in the three isotherms indicate the reservation of hollow structures and empty cores during the functionalization process, suggesting that the empty cores were accessible. Barrett−Joyner−Halenda (BJH) pore size distributions indicate that the diameter of the mesopores narrowly ranges from 2.1 to 2.7 nm, which can allow 5-ALA loading and release through uniform-sized nanochannels.

Table 1. BET Surface Area, Pore Size, and Pore Volume

	surface area (m^2 g^{-1})	pore size (nm)	pore volume (cm^3 g^{-1})
HMSNPs	991.92	2.70	1.11
HMSNP-NH_2	690.00	2.30	0.88
HMSNP-PEG +FA	535.71	2.12	0.69

After the HMSNPs were grafted with primary amine, the pore size decreased from 2.70 nm for HMSNPs to 2.30 nm for HMSNP-NH_2. This change implies that the primary amine groups were grafted on not only outside surface of HMSNP-NH_2, but also internal surface of the nanochannels. The pore size did not significantly decrease after the conjugation of folic acid and PEG, suggesting that folic acid and PEG were mainly distributed on the external surface of HMSNP-PEG+FA. It is anticipated that the remaining amine groups inside the mesopores would be positively charged under neutral pH. The positively charged amine group provides electrostatic interaction with negatively charged 5-ALA through its carboxylic group[15,17] to withhold 5-ALA in HMSNPs for entering into cancer cells. Under acidic intracellular environment of cancer cells, the carboxylic group becomes neural, and the electrostatic interaction is weakened. Thus, accelerated release of 5-ALA inside cancer cells is expected.

Generally, the decomposition rate of PphIX inside cancer cells (12−24 h) is 6 times higher than that in healthy cells (2−4 h),[29] which can be explained by the malfunction of the feedback mechanism in cancer cells. Furthermore, cancer cells usually have a low concentration of iron ions, an important catalyst for PphIX conversion, contributing to high accumulation of PphIX in cancer cells.[30] Although higher accumulation of PphIX inside cancer cells is normally expected as compared with that in healthy cells, the purpose of targeted 5-ALA delivery is to minimize nonspecific delivery and to avoid side-effects induced by the prerelease, thus enhancing the conversion efficiency of delivered 5-ALA. The targeted delivery capability of the multifunctional HMSNPs was investigated by using normal HEK293 cells as a negative control with low FAR expression (FA−), and B16F10 skin cancer cells as a positive control with high FAR expression (FA+). In order to trace the intracellular location of HMSNPs, fluorescein isothiocyanate (FITC)-labeled HMSNPs with folic acid and PEG conjugation, noted as HMSNP(FITC)-PEG+FA, was evaluated first.

Both HEK293 and B16F10 cells were treated with HMSNP(FITC)-PEG+FA (50 μg mL^{-1}). After 6 h incubation, the cells were washed with phosphate buffered saline (PBS) and the cell nucleus was stained by 4′,6-diamidino-2-phenylindole (DAPI) before observation under confocal laser scanning microscopy (CLSM). Green fluorescent spots represent FTIC labeled HMSNPs and cell nucleus shows blue color given by DAPI (Figure 2a). As compared with

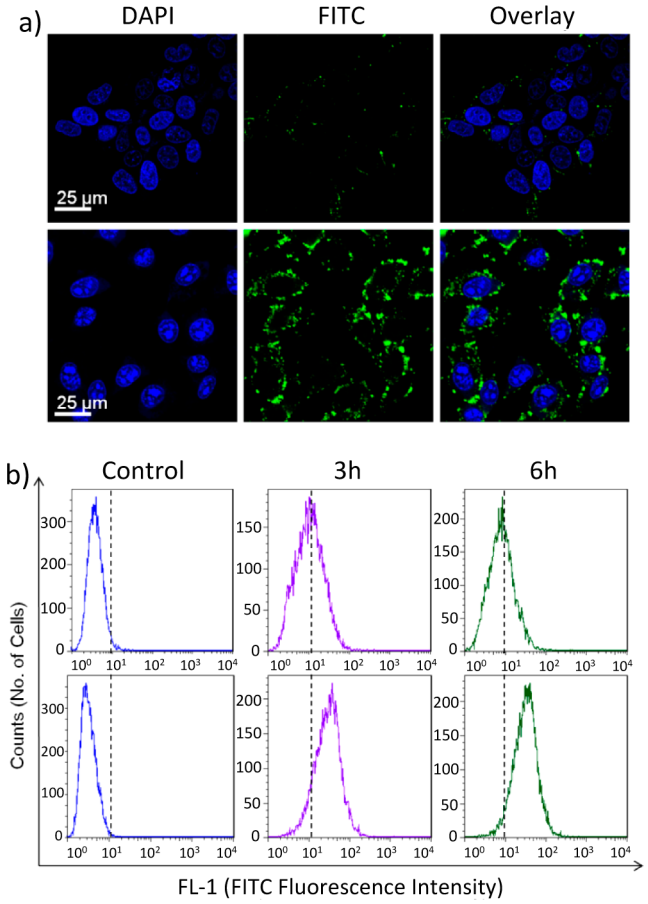

Figure 2. (a) CLSM images of HEK293 (up cell line) and B16F10 (bottom cell line) cells treated with HMSNP(FITC)-PEG+FA (50 μg mL^{-1}) for 6 h. Images from left to right are DAPI channel, FITC channel, and overlay of DAPI and FITC channels. (b) Flow cytometry results of HEK293 (up) and B16F10 (bottom) cells. Figures from left to right are cells without any treatment (control), and treated with HMSNP(FITC)-PEG+FA (50 μg mL^{-1}) for 3 and 6 h.

HEK293 cells (FA−), it could be observed that there was greater amount of green fluorescent spots inside B16F10 cells, indicating much higher uptake of HMSNP(FITC)-PEG+FA in B16F10 cells (FA+). Flow cytometry analysis further confirmed the CLSM results. For B16F10 cells (FA+), the histogram of FITC fluorescence intensity showed a significant right shift after the treatment with HMSNP(FITC)-PEG+FA (Figure 2b). For HEK293 cells (FA−), however, the histogram of FITC fluorescence intensity did not show obvious right shift (Figure 2b), suggesting much less uptake of HMSNP(FITC)-PEG+FA. Based on the CLSM and flow cytometry results, it can be concluded that HMSNP(FITC)-PEG+FA displays the capability of targeted delivery toward B16F10 cancer cells. Such targeted endocytosis of HMSNP(FITC)-PEG+FA to B16F10 cancer cells can be attributed to the FAR meditated endocytosis.[19,20]

5-ALA is a precursor of a strong photosensitizer, PphIX. Upon red light irradiation, PphIX can generate reactive singlet oxygen ($^1O_2$) that is highly toxic and eventually leads to cell apoptosis or necrosis. Thus, the generation and accumulation of PphIX in cancer cells are rather important, because PphIX is

DOI: 10.1021/acsami.5b03087
ACS Appl. Mater. Interfaces 2015, 7, 10671−10676

directly related to the PDT process. To investigate the PDT of PphIX, we seeded B16F10 cells in a T75 cell culture flask and cultured then for 24 h. After replacing the old medium with serum-free medium containing free 5-ALA (100 μg mL^{-1}), we further cultured the cells for 24 h for the PphIX formation. Dimethyl sulfoxide (DMSO, 3 mL) was then used to extract the generated PphIX. The optical property of the extracted DMSO solution was studied by using UV−vis and fluorescence spectroscopy. As seen from Figure 3a, characteristic UV−vis

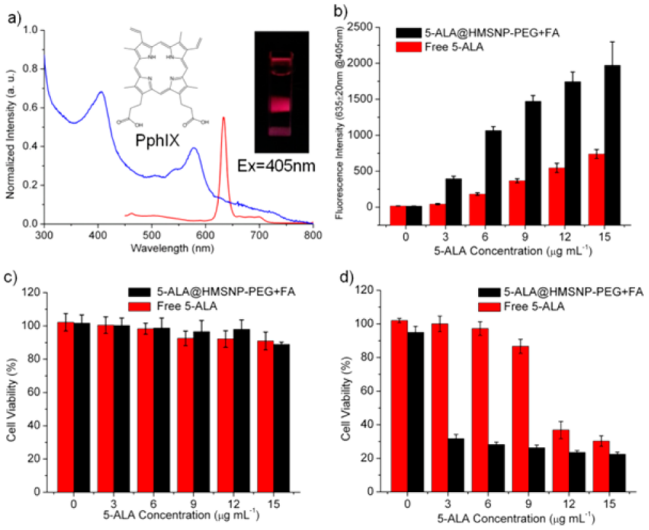

Figure 3. (a) Optical properties of PphIX extracted from B16F10 cancer cells; the blue curve is UV−vis absorption spectrum and the red curve is fluorescence emission spectrum. (b) PphIX generation by B16F10 cancer cells after being treated with 5-ALA@HMSNP-PEG +FA and free 5-ALA under equivalent concentrations of 5-ALA. MTS cell viability assay of B16F10 cancer cells after being treated with 5-ALA@HMSNP-PEG+FA and free 5-ALA under equivalent concentrations of 5-ALA (c) without and (d) with light irradiation at 635 nm for 15 min.

adsorption peaks of PphIX at 405 and 575 nm were observed. Upon 405 nm light excitation, strong red fluorescence emission at 635 nm was observed, which is characteristic fluorescence emission of PphIX. An optical photo of the fluorescence emission was shown as an inset image in Figure 3a, where a 405 nm light passed through the middle of the cuvette. Therefore, it was fully evident that PphIX could be generated in B16F10 cells by the administration of 5-ALA.

The in vitro PphIX generation was also investigated by CLSM. Both HEK293 and B16F10 cells were treated with 5-ALA@HMSNP-PEG+FA or free 5-ALA at a same amount of 5-ALA. After 24 h incubation, the cells were observed by CLSM. A 405 nm laser was used to excite the emission of generated PphIX. The detection channel ranges from 610 to 650 nm. Cells without any treatment were observed as a control. CLSM results are displayed in Figure 4, where red fluorescence color represents the presence of PphIX. In the case of HEK293 normal cells, red fluorescence color can hardly be observed (Figure 4b,c), which might be due to quick degradation rate of generated PphIX in normal cells as discussed above. For B16F10 skin cancer cells, obvious red fluorescence color was observed after the treatment with 5-ALA (Figure 4e). Even stronger red fluorescence was found for the B16F10 cells treated with 5-ALA@HMSNP-PEG+FA (Figure 4f) as compared with the case treated with free 5-ALA, indicating

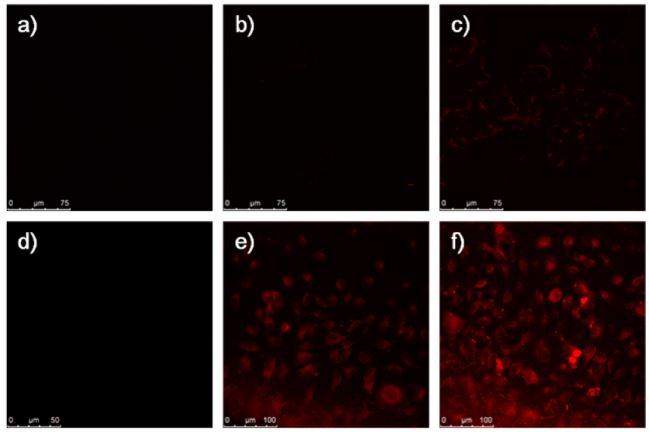

Figure 4. CLSM images of HEK293 normal cells (a) without any treatment, (b) treated with free 5-ALA (3.4 μg mL^{-1}), and (c) treated with 5-ALA@HMSNP-PEG+FA (100 μg mL^{-1}). CLSM images of B16F10 cells (d) without any treatment, (e) treated with free 5-ALA (3.4 μg mL^{-1}), and (f) treated with 5-ALA@HMSNP-PEG+FA (100 μg mL^{-1}). Scale bars: (a−c) 75, (d) 50, and (e, f) 100 μm.

that more PphIX was generated by using multifunctional HMSNPs as nanocarriers for the 5-ALA delivery.

A major purpose of using the nanocarriers for the 5-ALA delivery is to help 5-ALA bypass the lipophilic barrier to increase its cellular uptake in cancer cells. For free 5-ALA treatment, the cellular uptake of 5-ALA is based on free diffusion of small 5-ALA molecule, which is greatly limited by the lipophilic barrier. In the case of using multifunctional HMSNPs for the 5-ALA delivery, 5-ALA was first loaded inside the functional HMSNPs and transported into cancer cells via FAR meditated endocytosis, after which process the loaded 5-ALA was released inside cancer cells. Thus, enhanced 5-ALA uptake was observed by using multifunctional HMSNPs as the nanocarriers for the 5-ALA delivery, resulting in increased PphIX generation as observed in the CLSM studies (Figure 4). In addition, it is still necessary to quantify the amount of PphIX generated by the administration of 5-ALA@HMSNP-PEG+FA or free 5-ALA in order to statistically evaluate the PphIX generation. The generated amount of PphIX inside B16F10 cancer cells was measured indirectly by reading its fluorescence emission intensity. The excitation wavelength used was 405 nm, and the detection channel range was 635 ± 20 nm. From Figure 3b, a general trend of dose-dependent PphIX accumulation was observed for the cells treated with 5-ALA@HMSNP-PEG+FA or free 5-ALA. However, the fluorescence intensity increase by 5-ALA@HMSNP-PEG+FA is much higher than that of free 5-ALA. For the highest 5-ALA concentration used (15 μg mL^{-1}), the accumulation of PphIX by 5-ALA@HMSNP-PEG+FA was about 3 times higher than that by free 5-ALA, since the fluorescence intensity induced by 5-ALA@HMSNP-PEG+FA was around 2000 au, while the one by free 5-ALA was around 700 au

Next, the cell photocytotoxicity was investigated by 3-(4,5-dimethylthiazol-2-yl)-5-(3-carboxymethoxyphenyl)-2-(4-sulfophenyl)-2H-tetrazolium (MTS) assay. The dark toxicity of 5-ALA@HMSNP-PEG+FA and free 5-ALA was first evaluated. As shown in Figure 3c, without light irradiation, a negligible toxicity was found for both samples even at the highest concentration (15 μg mL^{-1}), indicating good biocompatibility of the multifunctional HMSNPs. Upon light irradiation at 635 nm (25 mW cm^{-2}) for 15 min, the cell viability decreased upon

DOI: 10.1021/acsami.5b03087
ACS Appl. Mater. Interfaces 2015, 7, 10671−10676

increasing the 5-ALA concentration for both 5-ALA@HMSNP-PEG+FA and free 5-ALA, suggesting effective cancer killing capability by the generation of toxic singlet oxygen in B16F10 cells (Figure 3d). By using HMSNP-PEG+FA to deliver 5-ALA, the cell viability decreased to about 30% at relatively lower 5-ALA concentration (3 μg mL^{-1}). For free 5-ALA, comparable cancer killing effect could only be achieved at relatively higher 5-ALA concentration (12 μg mL^{-1}). Thus, the enhanced photocytotoxicity by using 5-ALA@HMSNP-PEG+FA is consistent with the increased PphIX generation in B16F10 cells (Figure 3b). The MTS results clearly demonstrate that the multifunctional HMSNPs could serve as effective nanocarriers to deliver 5-ALA for the treatment of B16F10 skin cancer cells.

In summary, multifunctional hollow mesoporous silica nanoparticles (HMSNPs) containing PEG and folic acid targeting ligand have been successfully fabricated for targeted 5-ALA delivery and photodynamic therapy (PDT) against B16F10 skin cancer cells. Through folic acid receptor meditated endocytosis by using the multifunctional HMSNPs as the nanocarriers, the cellular uptake of 5-ALA and PphIX accumulation were significantly enhanced. Upon red light irradiation for PDT, efficient cancer cell killing effect from 5-ALA loaded HMSNPs (5-ALA@HMSNP-PEG+FA) was demonstrated. Therefore, the multifunctional HMSNP based 5-ALA delivery system presents a promising potential in practical skin cancer treatment.

■ ASSOCIATED CONTENT

Supporting Information

Additional synthesis and characterization data. The Supporting Information is available free of charge on the ACS Publications website at DOI: 10.1021/acsami.5b03087.

■ AUTHOR INFORMATION

Corresponding Author

*E-mail: zhaoyanli@ntu.edu.sg.

Notes

The authors declare no competing financial interest.

■ ACKNOWLEDGMENTS

This research is supported by the National Research Foundation (NRF), Prime Minister's Office, Singapore, under its NRF Fellowship (NRF2009NRF-RF001-015) and Campus for Research Excellence and Technological Enterprise (CREATE) Programme—Singapore Peking University Research Centre for a Sustainable Low-Carbon Future, the NTU-A*STAR Silicon Technologies Centre of Excellence under the program Grant 1123510003, as well as the NTU-Northwestern Institute for Nanomedicine.

■ REFERENCES

(1) Robertson, C. A.; Evans, D. H.; Abrahamse, H. Photodynamic Therapy (PDT): A Short Review on Cellular Mechanisms and Cancer Research Applications for PDT. *J. Photochem. Photobiol., B* **2009**, *96*, 1–8.

(2) Fakhar-e-Alam, M.; Rahim, S.; Atif, M.; Aziz, M. H.; Malick, M. I.; Zaidi, S. S. Z.; Suleman, R.; Majid, A. ZnO Nanoparticles as Drug Delivery Agent for Photodynamic Therapy. *Laser Phys. Lett.* **2014**, *11*, 025601.

(3) Xuan, S.-h.; Lee, S.-F.; Lau, J. T.-F.; Zhu, X.; Wang, Y.-X. J.; Wang, F.; Lai, J. M. Y.; Sham, K. W. Y.; Lo, P.-C.; Yu, J. C.; Cheng, C. H. K.; Leung, K. C.-F. Photocytotoxicity and Magnetic Relaxivity Responses of Dual-Porous γ-Fe_2O_3@Meso-SiO_2 Microspheres. *ACS Appl. Mater. Interfaces* **2012**, *4*, 2033–2040.

(4) Castano, A. P.; Demidova, T. N.; Hamblin, M. R. Mechanisms in Photodynamic Pherapy: Part Two—Cellular Signaling, Cell Metabolism and Modes of Cell Death. *Photodiagn. Photodyn. Ther.* **2005**, *2*, 1–23.

(5) Agostinis, P.; Berg, K.; Cengel, K. A.; Foster, T. H.; Girotti, A. W.; Gollnick, S. O.; Hahn, S. M.; Hamblin, M. R.; Juzeniene, A.; Kessel, D.; Korbelik, M.; Moan, J.; Mroz, P.; Nowis, D.; Piette, J.; Wilson, B. C.; Golab, J. Photodynamic Therapy of Cancer: An Update. *CA—Cancer J. Clin.* **2011**, *61*, 250–281.

(6) Peng, Q.; Warloe, T.; Berg, K.; Moan, J.; Kongshaug, M.; Giercksky, K. E.; Nesland, J. M. 5-Aminolevulinic Acid-based Photodynamic Therapy. Clinical Research and Future Challenges. *Cancer* **1997**, *79*, 2282–308.

(7) Pottier, R. H.; Chow, Y. F. A.; LaPlante, J. P.; Truscott, T. G.; Kennedy, J. C.; Beiner, L. A. Non-Invasive Technique for Obtaining Fluorescence Exication and Emssion Spectra *In Vivo*. *Photochem. Photobiol.* **1986**, *44*, 679–687.

(8) Kennedy, J. C.; Pottier, R. H.; Pross, D. C. Photodynamic Therapy with Endogenous Protoporphyrin IX: Basic Principles and Present Clinical Experience. *J. Photochem. Photobiol., B* **1990**, *6*, 143–148.

(9) da Silva, C. L.; Del Ciampo, J. O.; Rossetti, F. C.; Bentley, M. V. L. B.; Pierre, M. B. R. Improved *In Vitro* and *In Vivo* Cutaneous Delivery of Protoporphyrin IX from PLGA-Based Nanoparticles. *Photochem. Photobiol.* **2013**, *89*, 1176–1184.

(10) Ding, H.; Sumer, B. D.; Kessinger, C. W.; Dong, Y.; Huang, G.; Boothman, D. A.; Gao, J. Nanoscopic Micelle Delivery Improves the Photophysical Properties and Efficacy of Photodynamic Therapy of Protoporphyrin IX. *J. Controlled Release* **2011**, *151*, 271–277.

(11) Peng, Q.; Warloe, T.; Moan, J.; Godal, A.; Apricena, F.; Giercksky, K. E.; Nesland, J. M. Antitumor Effect of 5-Aminolevulinic Acid-Mediated Photodynamic Therapy Can Be Enhanced by the Use of a Low Dose of Photofrin in Human Tumor Xenografts. *Cancer Res.* **2001**, *61*, 5824–32.

(12) Friesen, S. A.; Hjortland, G. O.; Madsen, S. J.; Hirschberg, H.; Engebraten, O.; Nesland, J. M.; Peng, Q. 5-Aminolevulinic Acid-Based Photodynamic Detection and Therapy of Brain Tumors. *Int. J. Oncol.* **2002**, *21*, 577–82.

(13) Peng, Q.; Berg, K.; Moan, J.; Kongshaug, M.; Nesland, J. M. 5-Aminolevulinic Acid-Based Photodynamic Therapy: Principles and Experimental Research. *Photochem. Photobiol.* **1997**, *65*, 235–251.

(14) Szőcs, K.; Csík, G.; Kaposi, A. D.; Fidy, J. *In Situ* Detection of ALA-Stimulated Porphyrin Metabolic Products in Escherichia Coli B by Fluorescence Line Narrowing Spectroscopy. *Biochim. Biophys. Acta Mol. Cell Res.* **2001**, *1541*, 170–178.

(15) Oo, M. K.; Yang, X.; Du, H.; Wang, H. 5-Aminolevulinic Acid-Conjugated Gold Nanoparticles for Photodynamic Therapy of Cancer. *Nanomedicine* **2008**, *3*, 777–86.

(16) Shaker, M.; Ramadan, H.; Mohamed, M.; El khatib, A.; Roston, G. Enhanced Photodynamic Efficacy of PLGA-Encapsulated 5-ALA Nanoparticles in Mice Bearing Ehrlich Ascites Carcinoma. *Appl. Nanosci.* **2014**, *4*, 777–789.

(17) Chung, C. W.; Chung, K. D.; Jeong, Y. I.; Kang, D. H. 5-Aminolevulinic Acid-Incorporated Nanoparticles of Methoxy Poly-(Ethylene Glycol)-Chitosan Copolymer for Photodynamic Therapy. *Int. J. Nanomed.* **2013**, *8*, 809–819.

(18) Ma, X.; Teh, C.; Zhang, Q.; Borah, P.; Choong, C.; Korzh, V.; Zhao, Y. Redox-Responsive Mesoporous Silica Nanoparticles: A Physiologically Sensitive Codelivery Vehicle for siRNA and Doxorubicin. *Antioxid. Redox Signal.* **2014**, *21*, 707–722.

(19) Luo, Z.; Ding, X.; Hu, Y.; Wu, S.; Xiang, Y.; Zeng, Y.; Zhang, B.; Yan, H.; Zhang, H.; Zhu, L.; Liu, J.; Li, J.; Cai, K.; Zhao, Y. Engineering a Hollow Nanocontainer Platform with Multifunctional Molecular Machines for Tumor-Targeted Therapy *in Vitro* and *in Vivo*. *ACS Nano* **2013**, *7*, 10271–10284.

DOI: 10.1021/acsami.5b03087
ACS Appl. Mater. Interfaces 2015, 7, 10671–10676

(20) Ma, X.; Zhao, Y.; Ng, K. W.; Zhao, Y. Integrated Hollow Mesoporous Silica Nanoparticles for Target Drug/siRNA Co-Delivery. *Chem.—Eur. J.* **2013**, *19*, 15593−15603.
(21) Doucette, M. M.; Stevens, V. L. Folate Receptor Function Is Regulated in Response to Different Cellular Growth Rates in Cultured Mammalian Cells. *J. Nutr.* **2001**, *131*, 2819−2825.
(22) Zhang, Q.; Wang, X.; Li, P.-Z.; Nguyen, K. T.; Wang, X.-J.; Luo, Z.; Zhang, H.; Tan, N. S.; Zhao, Y. Biocompatible, Uniform, and Redispersible Mesoporous Silica Nanoparticles for Cancer-Targeted Drug Delivery *In Vivo*. *Adv. Funct. Mater.* **2014**, *24*, 2450−2461.
(23) Fang, X.; Chen, C.; Liu, Z.; Liu, P.; Zheng, N. A Cationic Surfactant Assisted Selective Etching Strategy to Hollow Mesoporous Silica Spheres. *Nanoscale* **2011**, *3*, 1632−1639.
(24) Greish, K. Enhanced Permeability and Retention (EPR) Effect for Anticancer Nanomedicine Drug Targeting. In *Cancer Nanotechnology*, Grobmyer, S. R., Moudgil, B. M., Eds.; Humana Press: New York, 2010; Chapter 3, pp 25−37.
(25) Ma, X.; Ong, O. S.; Zhao, Y. Dual-Responsive Drug Release from Oligonucleotide-Capped Mesoporous Silica Nanoparticles. *Biomater. Sci.* **2013**, *1*, 912−917.
(26) Coates, J. Interpretation of Infrared Spectra, A Practical Approach. In *Encyclopedia of Analytical Chemistry*; John Wiley & Sons: New York, 2006.
(27) Shameli, K.; Bin Ahmad, M.; Jazayeri, S. D.; Sedaghat, S.; Shabanzadeh, P.; Jahangirian, H.; Mahdavi, M.; Abdollahi, Y. Synthesis and Characterization of Polyethylene Glycol Mediated Silver Nanoparticles by the Green Method. *Int. J. Mol. Sci.* **2012**, *13*, 6639−6650.
(28) Song, Y.; Shi, W.; Chen, W.; Li, X.; Ma, H. Fluorescent Carbon Nanodots Conjugated with Folic Acid for Distinguishing Folate-Receptor-Positive Cancer Cells from Normal Cells. *J. Mater. Chem.* **2012**, *22*, 12568−12573.
(29) Steluti, R.; De Rosa, F. S.; Collett, J.; Tedesco, A. C.; Bentley, M. V. L. B. Topical Glycerol Monooleate/Propylene Glycol Formulations Enhance 5-Aminolevulinic Acid *in Vitro* Skin Delivery and *in Vivo* Protophorphyrin IX Accumulation in Hairless Mouse Skin. *Eur. J. Pharm. Biopharm.* **2005**, *60*, 439−444.
(30) Grimbergen, M. C.; van Swol, C. F.; Jonges, T. G.; Boon, T. A.; van Moorselaar, R. J. Reduced Specificity of 5-ALA Induced Fluorescence in Photodynamic Diagnosis of Transitional Cell Carcinoma after Previous Intravesical Therapy. *Eur. Urol.* **2003**, *44*, 51−56.

DOI: 10.1021/acsami.5b03087
ACS Appl. Mater. Interfaces 2015, 7, 10671−10676